Overcoming the screening-induced performance limits of nanowire biosensors: a simulation study on the effect of electro-diffusion flow

Yang Liu[1], Klas Lilja[2], Clemens Heitzinger[3], Robert W. Dutton[1]

[1]Center for Integrated Systems, Stanford University, Stanford, CA 94305, USA
[2]Robust Chip Inc., Pleasanton, CA 94588, USA
[3]Dept. of Math. & Wolfgang Pauli Inst., University of Vienna, A-1090 Vienna, Austria
Phone: (650)723-9796, E-mail: yangliu@gloworm.stanford.edu

Abstract

Device-level simulation capabilities have been developed to self-consistently model the Si-nanowire (NW) biosensor systems. Our numerical study demonstrates that by introducing electro-diffusion current flow in the electrolyte solutions, the electrostatic screening of the biological charge can be significantly suppressed; an improvement of the sensed signal strength by >≈10X is indicated. Based on such an operation principle, the screening-induced performance limits on Si-NW biosensors can be overcome.

Introduction

Recently, ISFET-type devices [1,2] using silicon nanowires (Si-NWs) have attracted enormous research interest for label-free detection of charged biological species (DNAs or proteins) [3-6]. Their operation principle is illustrated in Fig. 1(a): the selective binding of the analytes (target complementary ssDNA or antigens) to the receptors (primary ssDNA or antibodies) on the Si-NW surface modulates the NW surface potential through a field effect, which produces signals in terms of its conductance change. For such types of biosensors, the electrolyte screening has usually been regarded as a detrimental factor that limits the ultimate sensitivity [1, 2]. In particular, a recent study raised further attention to such a performance limit in Si-NW sensors [7, 8]. The underlying physics is the Debye-Huckel screening behavior of counter-ions around the biological charge, which leads to an exponential decay of the induced potential change. In this work, we demonstrate device-level simulation capabilities to self-consistently model the Si-NW biosensor systems. Using the developed simulation capabilities, we investigate how the charge screening behavior is affected by introducing steady-state electro-diffusion current flow in the electrolyte solutions. It is demonstrated that the screening of the biological charge can be significantly suppressed under such quasi-equilibrium conditions; an improvement of Si-NW signal strength by >≈10X is indicated under an external electric field of ≈100 kV/cm. Based on the proposed operation principle, screening-induced performance limits of Si-NW biosensors can be overcome.

Operation Principle and Model Equations

Fig. 1(b) illustrates the proposed detection scheme: instead of the usual scheme where only a reference solution electrode is used, two biased electrodes are used to introduce flow of the mobile ions around the Si-NWs. This scheme changes the screening behavior as further illustrated in Fig. 2. In the equilibrium case (a), when a negative biological charge -Q is introduced near the NW native oxide layer (≈1-2 nm thick), counter-ions accumulate in the vicinity and effectively shield that charge. The Debye-Huckel theory gives a Debye length $1/\kappa$≈1 nm for a 0.1 M electrolyte concentration that is close to the physiological condition. It dictates that the biological charge cannot be detected beyond a few Debye lengths. An equivalent circuit plot is given for further illustration, where among the various capacitances Csc is due to screening and Cd/Ci/Ca are for NW depletion, inversion, and accumulation regimes, respectively. The total image charge Q=Q'+Q'' is divided among the competing capacitances: only Q' induced in the Si-NW contributes to its conductance change. In the case of electro-diffusion flow (b), the screening behavior is qualitatively different: the detailed balance between drift and diffusion is no longer imposed and the Debye-Huckel screening limited case no longer dominates in such a quasi-equilibrium case. As clarified in [9], the general screening behavior in this case is the superposition of an Ohmic type and the Debye-Huckel type. Correspondingly, the screening capacitance Csc is dramatically reduced, which in turn leads to the increase of Q'.

Some recent efforts on simulating Si-NW biosensors have been reported [7, 8, 10]; but only the equilibrium electrolytes

1-4244-2377-4/08/$20.00 ©2008 IEEE

were modeled by solving the Poisson-Boltzmann equation. The modeling equations used in this work are described in Table 1. We simulate a segment of Si-NW that contains one DNA binding site. The ion transport is modeled by the Poisson-Nernst-Planck (PNP) equations. The Si electron and hole densities are calculated under an assumption of low S/D biases, which is a reasonable measurement condition [5]. The electron/hole quasi-Fermi levels also account for both the electrode reference energy and the affinity difference between Si and electrolyte solutions [11]. All the model equations in the different regions are solved self-consistently over 3-D device structures using a general device simulator, PROPHET [12]. In the following, we present simulation studies of two biosensor device geometries; both show consistent results.

Simulation Results and Discussions

Electrolyte-Insulator-Metal (EIM): The grounded metal in this planar EIM structure is covered with 1 nm thick oxide. The binding of a 12-base-pair DNA strand at the center is examined. Its double-helix structure and backbone charge are spatially resolved to 2 Angstrom in a 3-D mesh. The electrolyte bias (Va) is applied across the left and right boundaries (distance 80 nm). The simulated differences in electrostatic potential and cation concentration between the cases with and without the DNA are plotted in Fig. 3 & 4, respectively. Compared to the zero-bias case (a), applying 1 V bias (b) results in significantly more spreading of the cation screening layer. The vertical electric field at the bottom ground plane is plotted in Fig. 5. This quantity is proportional to the surface density of the induced charge in the metal. At 1 V, the non-zero electric field induces charge over a broader area of the metal plane. The total induced charge Q' is calculated by integrating the displacement flux over the bottom plane. Fig. 6 plots the fraction of induced charge at various conditions. At 0 V, only a small fraction of the DNA charge Q0 is collected. However, as the bias increases, Q' increases rapidly without being screening-limited. At 3 V bias and 20 mM concentration, this fraction is boosted by about 10X.

Si-NW: The mesh used for simulations of a 10 nm long, 10 nm diameter Si-NW segment is shown in Fig. 7. The NW is p-doped at 1E18/cm^3. The DNA is approximated by a small, impermeable rod with the backbone charge uniformly distributed for simplicity, although in principle its realistic geometry can be resolved as in the EIM case. The distance between the two side electrodes is 100 nm. A cross-sectional plot of the potential difference between the ssNDA and dsDNA cases is given in Fig. 8. At 0 V, the potential change only occurs close to the DNA, indicating a Debye-Huckel screening. At 1 V, it spreads over a much broader space and penetrates more into the Si-NW region. We also note the potential variation in Si-NW, which means the assumption of equipotential NW surfaces in [7, 8] is generally over-simplified. This is because the electrolyte concentration (0.1 M=6.02E19/cm^3) is high compared to NW doping; it is therefore necessary to model the Si-NW as semiconductor instead of as metallic. The induced charge Q' is plotted for different biases and electrolyte concentrations in Fig. 9. At low biases, Q' is only about 50% of the total doping charge, indicating the Si-NW is in a slight depletion mode. At higher external fields, Q' quickly increases and the accumulation mode is reached. The relative Si-NW conductance change due to hybridization is plotted in Fig. 10. This quantity is proportional to dQ'/Q0', where dQ' is the difference of Q' between ssDNA and dsDNA cases; and Q0' is the NW charge in the ssDNA case at 0V. At 0 V, the conductance change is screening-limited to 2% and 7% for 100 mM and 10 mM solutions, respectively. Such a limit is overcome by increasing biases. At 1 V (corresponding to 100 kV/cm field strength), enhancement factors of 11X and 8X are observed for the two solutions respectively.

Summary

We have demonstrated device-level simulation capabilities to study the role of screening in Si-NW biosensors. It is shown that by introducing electro-diffusion flow, the screening is greatly suppressed and screening-induced performance limits can be overcome.

Acknowledgement

Useful discussions with Dr. A. Talasaz at Stanford are appreciated. We also thank Prof. P. H.-S. Wong at Stanford for computing resources. CH was supported by the Austrian Academy of Sciences jubilee-fund project "Multi-Scale Modeling and Simulation of Field-Effect Nano-Biosensors."

References

[1] P. Bergveld, Sensors and Actuators B, 88, p.1, 2003;
[2] M. Schoning and A. Poghossian, Analyst, 127, p.1137, 2002;
[3] J. Hahm and C. Lieber, Nano Lett., 4, p.51, 2004;
[4] Z. Li et al, Nano Lett., 4, p.245, 2004;
[5] M.M. Cheung et al, Curr. Opin. Chem. Biol., 10, p.11, 2006;
[6] E. Stern et al, Nature, 445, p.519, 2007
[7] P. Nair and M. Alam, IEEE T-ED, 54, p.3400, 2007;
[8] P. Nair and M. Alam, Nano Lett., 8, p.1281, 2008;
[9] Y. Liu, J. Sauer and R.W. Dutton, J. Appl. Phys., 103, p.84701, 2008;
[10] C. Heitzinger and G. Klimeck, J. Comp. Electron., 6, p.387, 2007;
[11] D. Landheer et al, J. Appl. Phys., 98, p.044701, 2005;
[12] http://www-tcad.stanford.edu/~prophet.

Table 1: Model equations used to simulate different regions of Si-NW biosensors. The potential is set to be continuous at interfaces. The oxide and biomolecule regions are impermeable to the ions. Dirichlet boundary conditions are used for potential and ion densities at the electrolyte electrodes. Neumann conditions with zero normal fluxes are used at the other simulation domain boundaries.

Si-NW	Electrolyte	Gate Oxide
$-\nabla\cdot(\varepsilon_{si}\nabla\psi) = q\left(p - n + N_{dop}\right)$, $p = n_i \exp\left(\frac{E_F - q\psi}{k_B T}\right)$, $n = n_i \exp\left(\frac{-E_F + q\psi}{k_B T}\right)$. E_F: quasi-Fermi level; n_i: 1e10/cm^3 ; ε_{si}: $11.9\varepsilon_0$.	$-\nabla\cdot(\varepsilon_w\nabla\psi) = q(C_+ - C_-)$, $\nabla\cdot(qD_+\nabla C_+ + \mu_+ qC_+\nabla\psi) = 0$, $\nabla\cdot(qD_-\nabla C_- - \mu_- qC_-\nabla\psi) = 0$. C_+: cation density; C_-: anion density; ε_w: $80\varepsilon_0$; μ_+: 7.62e-8 m^2/Vs; μ_-: 7.92e-8 m^2/Vs; D: $k_B T/q$.	$\nabla\cdot(\varepsilon_{ox}\nabla\psi) + \rho_f = 0$. ρ_f: fixed bulk & interface charge; ε_{ox}: $3.9\varepsilon_0$. **Biomolecule** $\nabla\cdot(\varepsilon_d\nabla\psi) + \rho_r = 0$. ε_d: $4\varepsilon_0$; ρ_r: fixed residue charge.

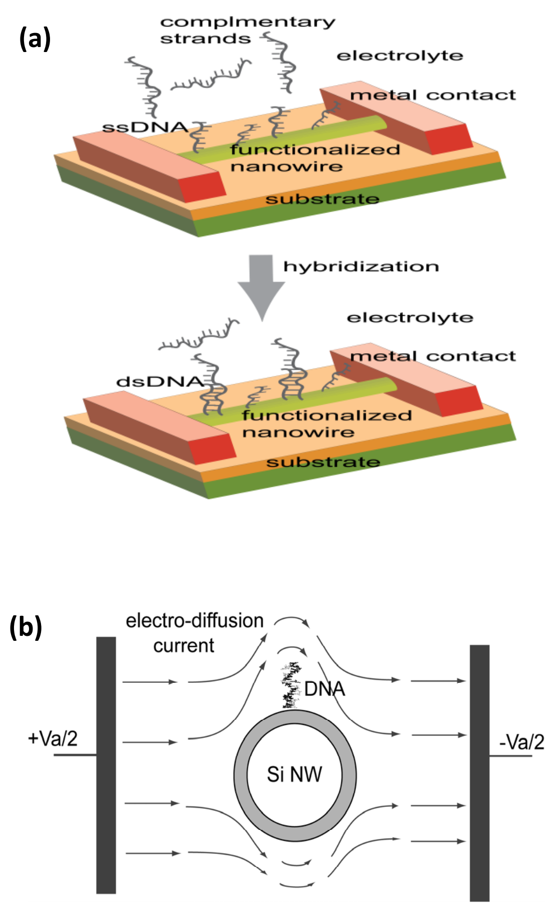

Fig. 1: (a) Operation of the biosensors: the Si-NW surfaces are functionalized with primary ssDNA as receptors; the subsequent hybridization of the target complementary ssDNAs modulates the Si-NW surface potential through a field effect, which produces signals in terms of NW conductance change. (b) The proposed detection scheme: two biased electrodes are used in electrolytes to introduce electro-diffusion flow of the mobile ions around NWs.

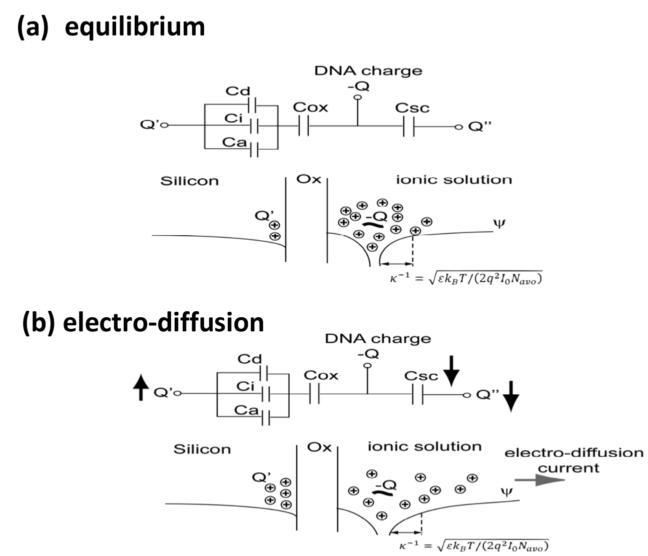

Fig. 2: Different screening behavior under (a) equilibrium and (b) electro-diffusion conditions. The equivalent circuits show charge partition between competing capacitances. The presence of electro-diffusion reduces Csc, which increases Q' and the NW conductance change.

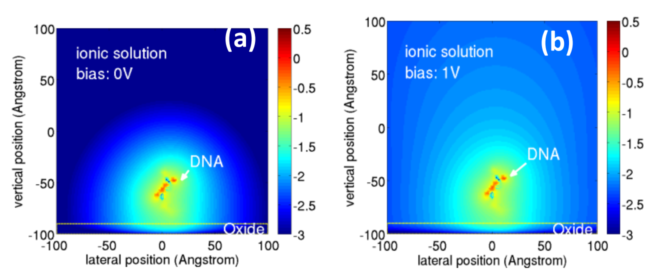

Fig. 3: Logarithmic magnitude of simulated potential change, log10(|dψ|), at vertical cut-plane of an EIM structure for (a) 0 V and (b) 1 V electrolyte biases. dψ (unit V) is obtained as the potential difference between the cases with or without a 12-bp DNA at center.

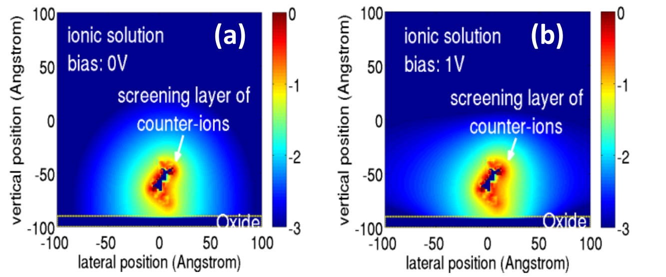

Fig. 4: Logarithmic magnitude of simulated cation density change, log10(dC+), at a vertical cut-plane of an EIM structure (same as Fig. 3) for (a) 0 V and (b) 1 V electrolyte biases. dC+ (unit: M) is obtained as difference between the cases with or without a 12-bp DNA at center.

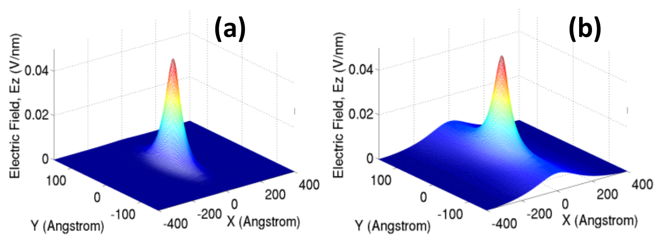

Fig. 5: Simulated vertical electric field at bottom metal plane of a structure (same as Fig. 3 & 4) for (a) 0 V and (b) 1 V biases. This quantity is proportional to the surface density of induced charge. At 1 V bias, charge is induced over a broader area of the metal plane.

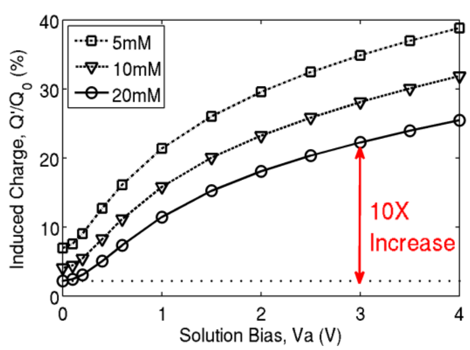

Fig. 6: Electrolyte bias dependence of induced charge Q' (normalized by DNA charge Q0) at 5, 10, and 20 mM electrolyte concentrations. At 3 V and 20 mM condition, an enhancement of ~10X compared to 0 V is found.

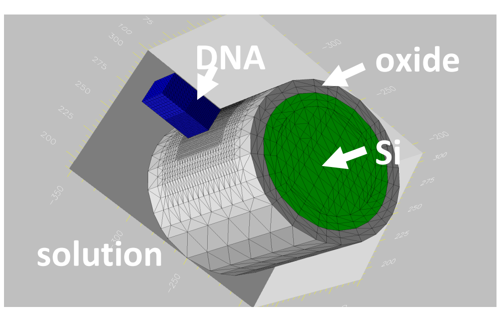

Fig. 7: 3-D mesh used for simulations of a 10 nm long, 10 nm diameter Si-NW segment with 1 nm thick native oxide. The DNA is approximated by a charged small rod. Electrolyte biases are applied at two sides as illustrated in Fig. 1(b).

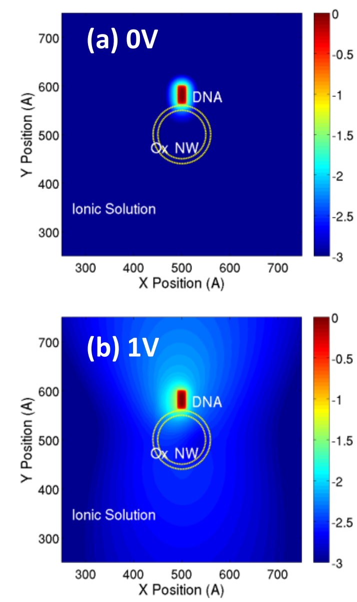

Fig. 8: Logarithmic magnitude of simulated potential change, log10(|dψ|), at a lateral cut-plane of Si-NW for (a) 0 V and (b) 1 V electrolyte biases. dψ (unit: V) is obtained as the potential difference between ssDNA and dsDNA cases.

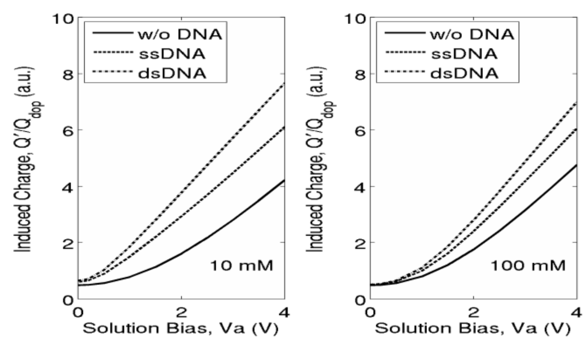

Fig. 9: Charge induced in Si-NW, Q' (normalized by NW doping charge) as functions of electrolyte biases for cases of no DNA, ssDNA, and dsDNA respectively. Two electrolyte concentrations, 10 mM and 100 mM, are examined.

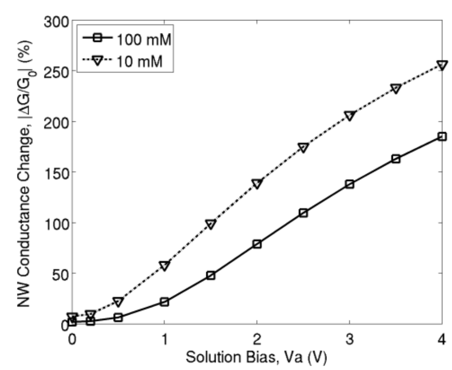

Fig. 10: Si-NW conductance change between ssDNA and dsDNA cases as functions of electrolyte biases. This quantity is normalized by G0 of the ssDNA case at 0 V. The conductance change improves as bias increases. At 1 V, enhancement factors of ~11X and ~8X are seen at 100 mM and 10 mM conditions, respectively.